Nanoscale

Supporting Information

Controlled Ligation and Elongation of Uniformly Truncated Amyloid Nanofibrils

Seokbeom Roh[a, b], Da Yeon Cheong[a, b], Sangwoo Lee[a], Jongsang Son[c], Insu Park*[, d], Gyudo Lee*[a, b]

a. Department of Biotechnology and Bioinformatics, Korea University, Sejong 30019, South Korea

b. Interdisciplinary Graduate Program for Artificial Intelligence Smart Convergence Technology, Korea University, Sejong 30019, South Korea

c. Department of Biomedical Engineering, New Jersey Institute of Technology, Newark, NJ 07102, United States

d. Department of Biomedical Engineering, Yonsei University, Wonju 26493, Republic of Korea

* Correspondence: I.P. (insu1023@gmail.com); G.L. (lkd0807@korea.ac.kr)

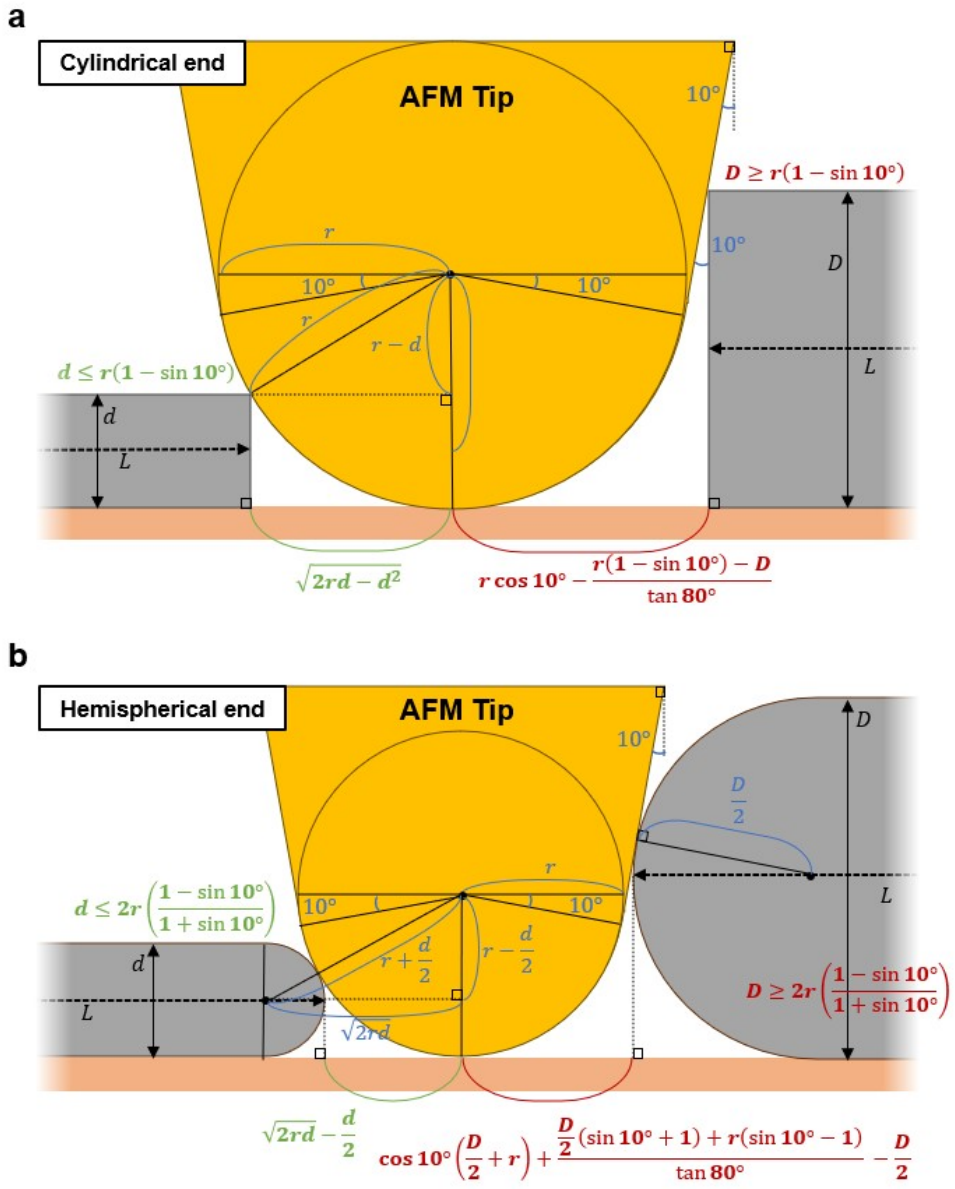

Figure S1. Schematic illustration of the AFM tip convolution effect on nanofibril length measurement depending on end shapes. The cases shown include nanofibrils with (a) cylindrical ends and (b) hemispherical ends. The diagram shows an AFM tip in the center, with a fibril on the left whose diameter is smaller than the effective tip radius and a fibril on the right whose diameter is larger than the effective tip radius. Given the AFM tip radius (7 nm) and the amyloid nanofibril diameter (2.8 nm), the estimated length error per end is 5.6 nm for cylindrical ends and 4.86 nm for hemispherical ends. Accounting for two fibril ends, the total length error ranges between 9.7–11.2 nm per fibril, corresponding to approximately 10% for ANF-100 and 5% for ANF-200. To ensure accurate measurement of nanofibril length, it is essential to account for the tip convolution effect.

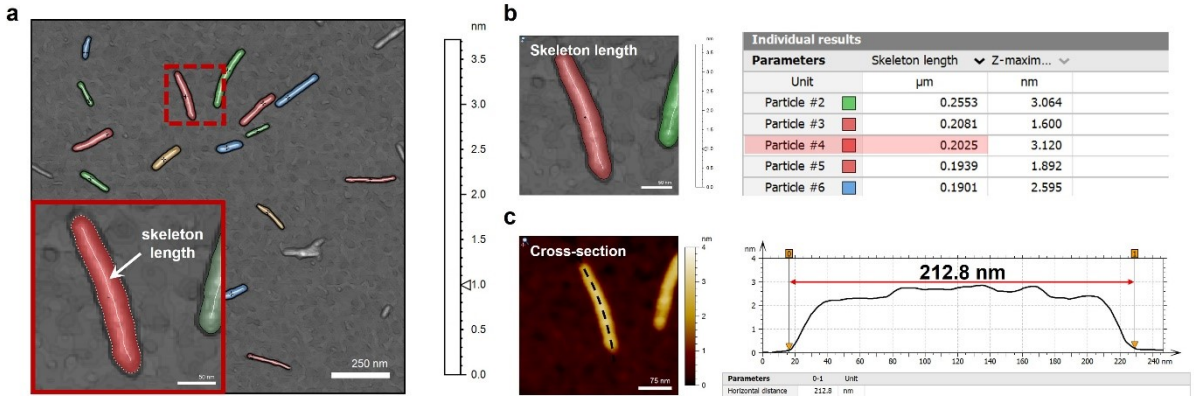

Figure S2. Comparison of results obtained from cross-sectional analysis and skeletonization-based particle analysis. (a) demonstrates the process of obtaining skeleton length using skeletonization in particle analysis. (b) Fibril length analysis results obtained using skeletonization-based particle analysis. (c) Fibril length measured via cross-sectional analysis.

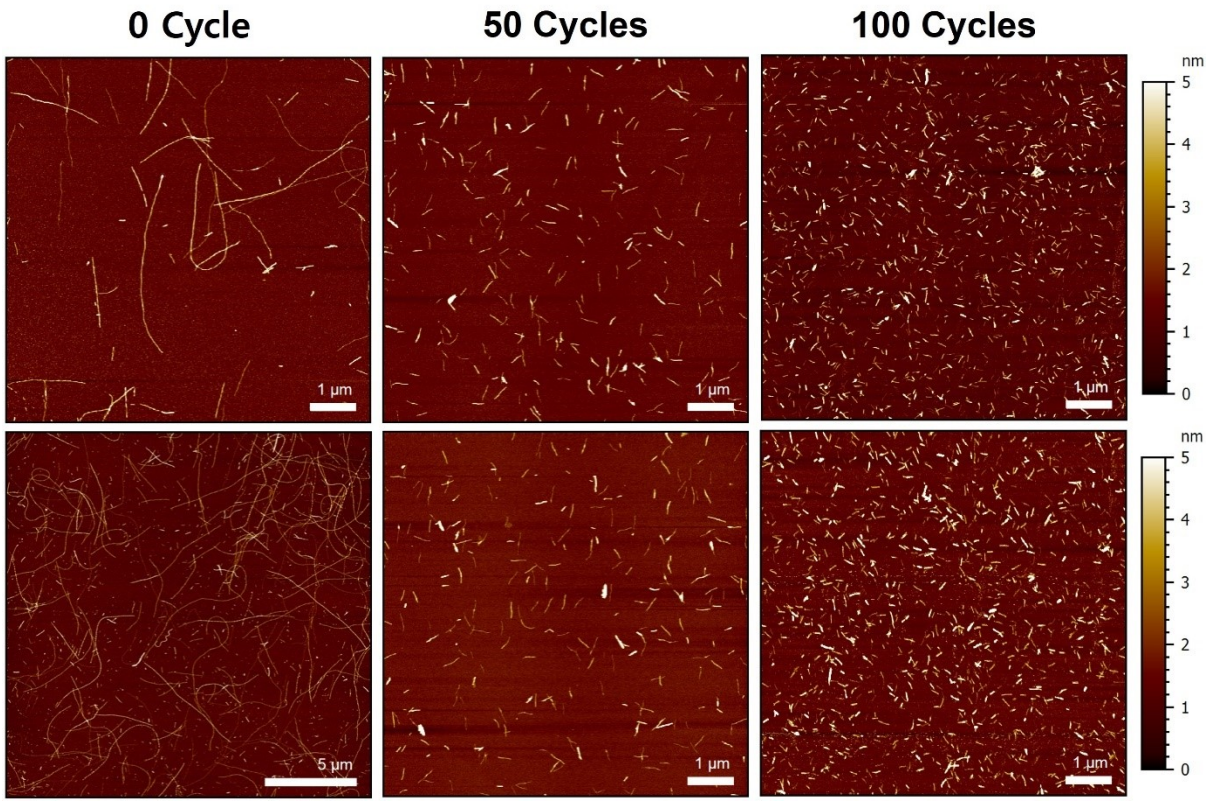

Figure S3. AFM images of amyloid nanofibrils after repeated extrusion through a carbonate filter with 200 nm pores, showing 0, 50, and 100 extrusion cycles.

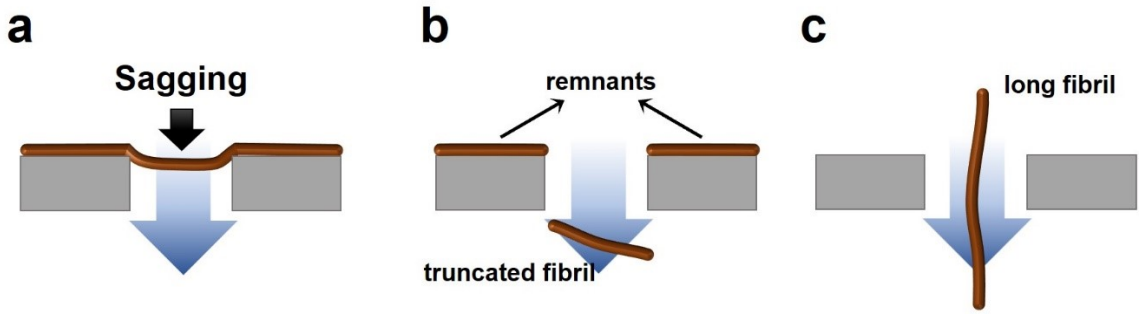

Figure S4. Schematic illustration of three factors that could cause fibrils larger than the pore size to emerge during extrusion. (a) fibrils sagging across the pore, (b) fibril remnants on filter after truncation, and (c) passing through pores

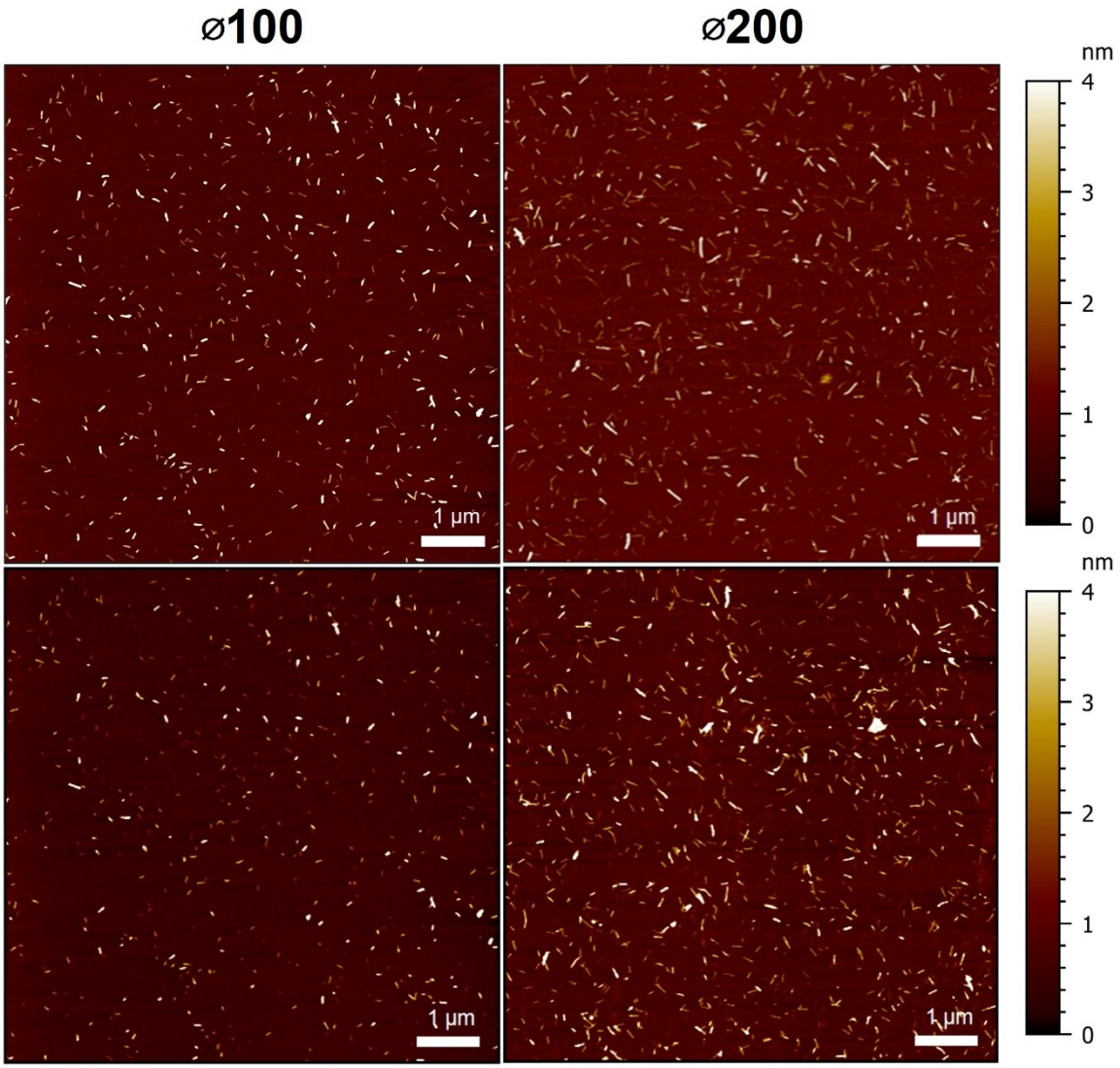

Figure S5. AFM images of amyloid nanofibrils after 100 extrusion cycles through carbonate filters with different pore sizes.

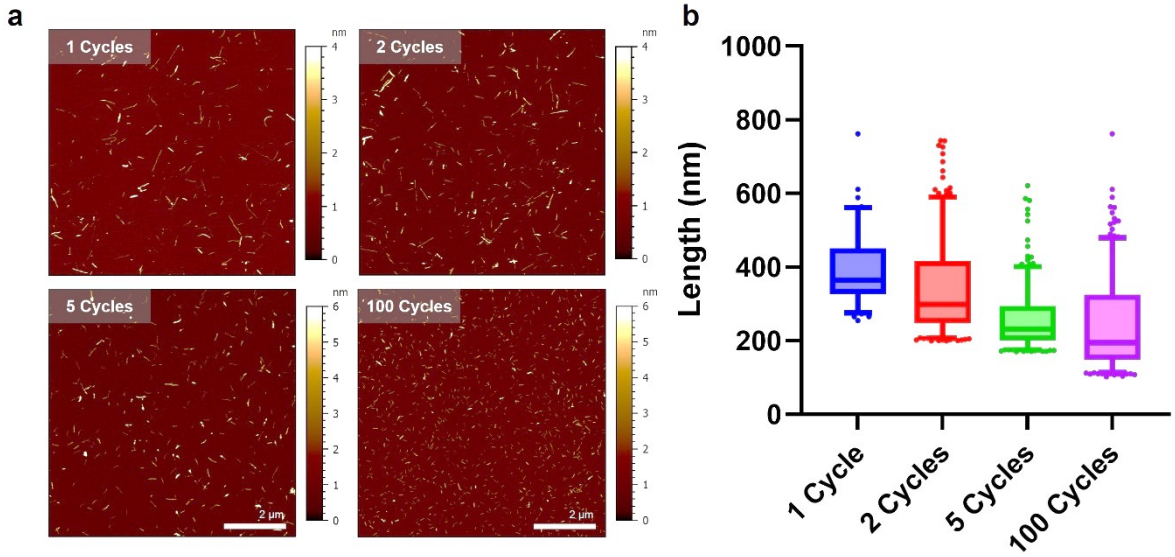

Figure S6. Analysis of amyloid nanofibril length after repeated extrusion through a carbonate filter with 400 nm pores. (a) AFM images of amyloid nanofibrils after 1 to 100 extrusion cycles through filters (b) Box-and-whisker plots show the distribution of fibril lengths, illustrating the interquartile range and median, with whiskers extending to 5%–95%.

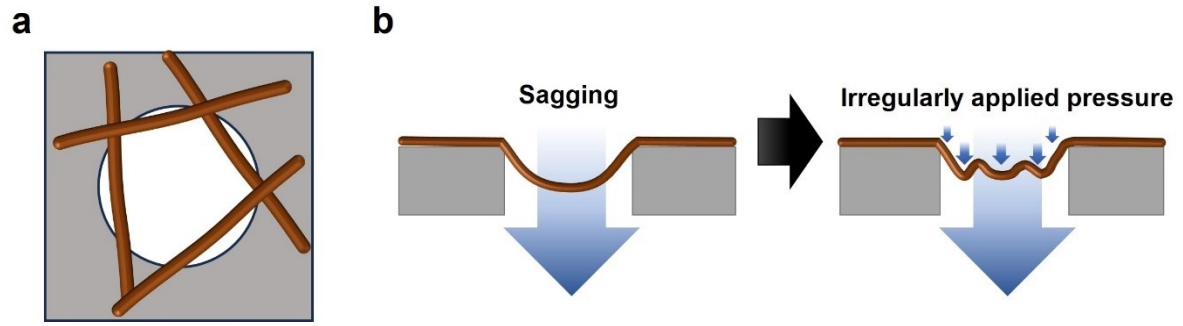

Figure S7. Schematic illustration of disadvantages of using bigger pores. (a) The pores of the wider filter are such that when the fibril is adsorbed to the filter, it hangs on the periphery of the pore rather than passing through the center of the pore. (b) The wider pores of the filter enhance the sagging of fibrils across the pores and apply uneven pressure.

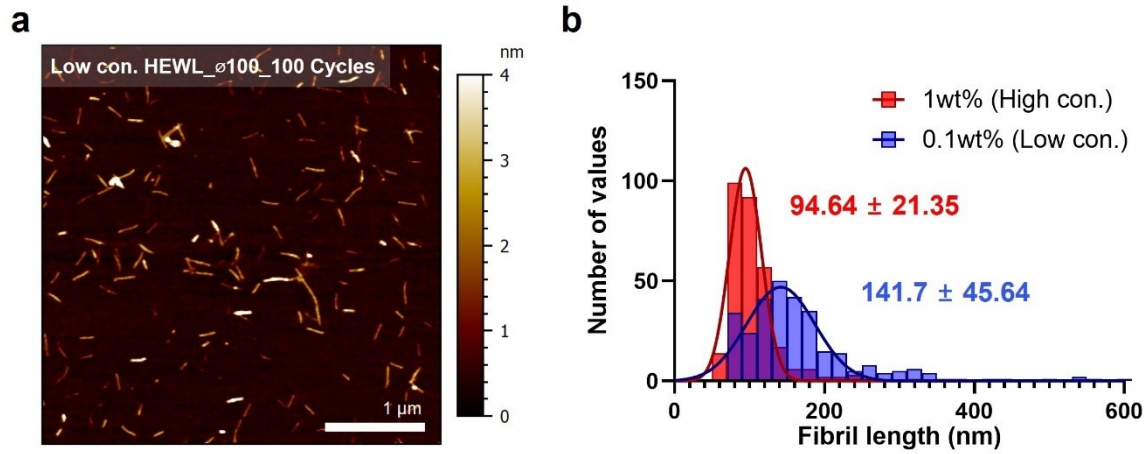

Figure S8. Analysis of amyloid nanofibril diameter and length after 100 cycles through carbonate filters with different pore sizes. (a) AFM image of low concentration of amyloid nanofibrils after 100 extrusion cycles through filters with pore sizes of 100 nm (b) Histograms display the distribution of fibril lengths fitted to a Gaussian model, with mean and standard deviation indicated.

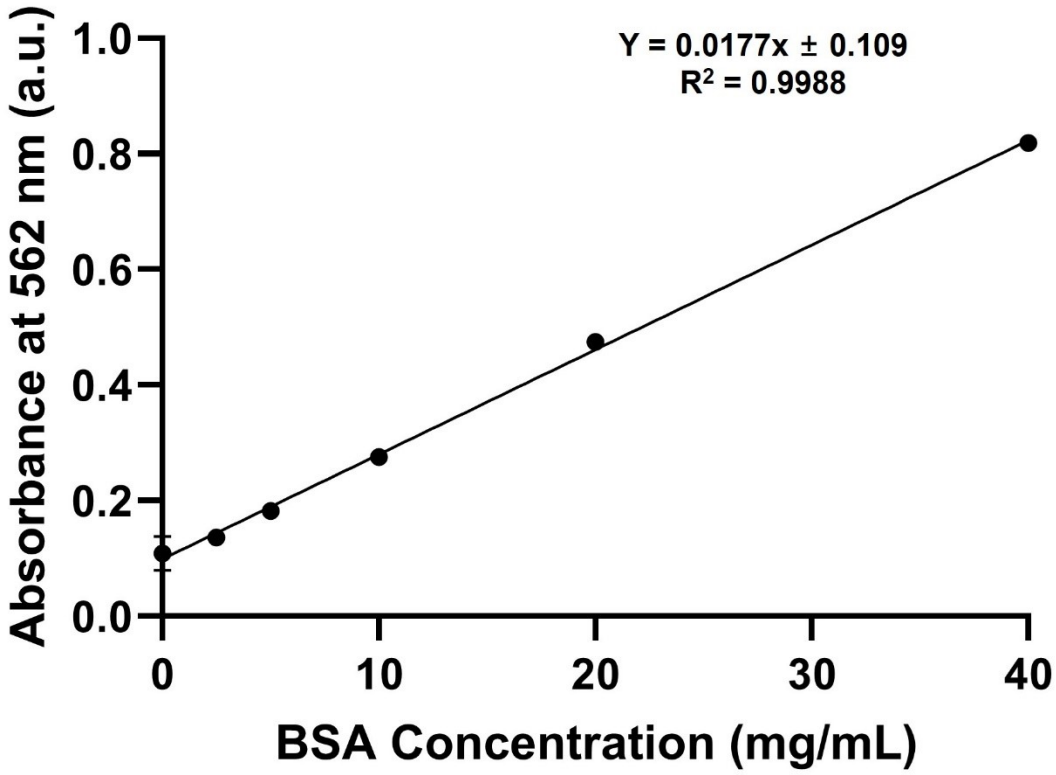

Figure S9. Calibration curve of standard protein (BSA) for absorbance at 562 nm, plotted as a function of concentration (mg/mL) with a linear regression fit (R^2 = 0.9988).

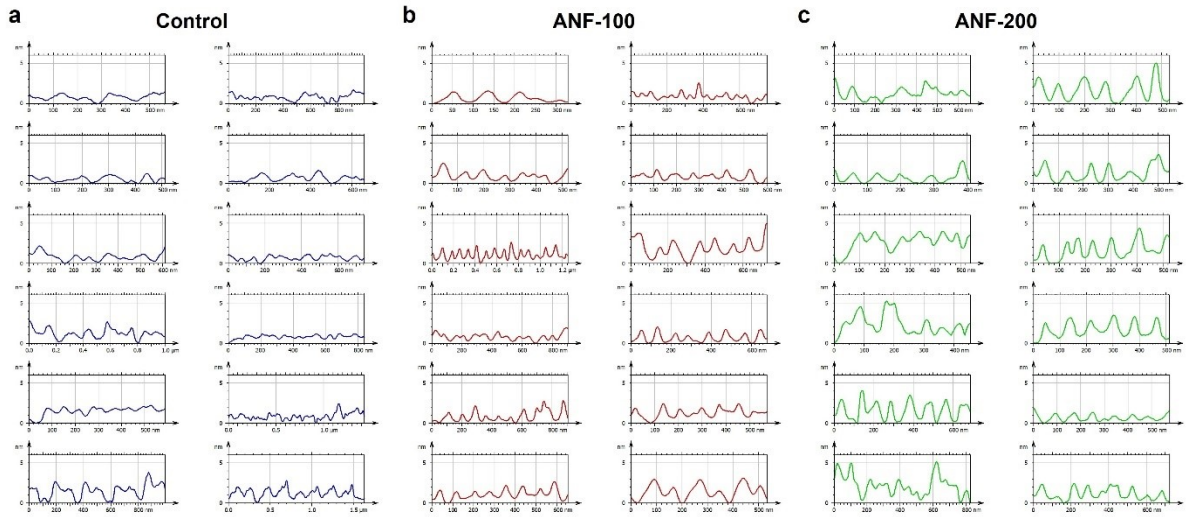

Figure S10. Representative cross-sectional profiles of uniformly truncated amyloid nanofibril morphology after incubation at 60°C for 2 weeks. Cross-sectional profiles were taken through the center of individual nanofibrils in each condition: (a) Control group, (b) ANF-100, and (c) ANF-200. The y-axis represents height in nanometers (nm).

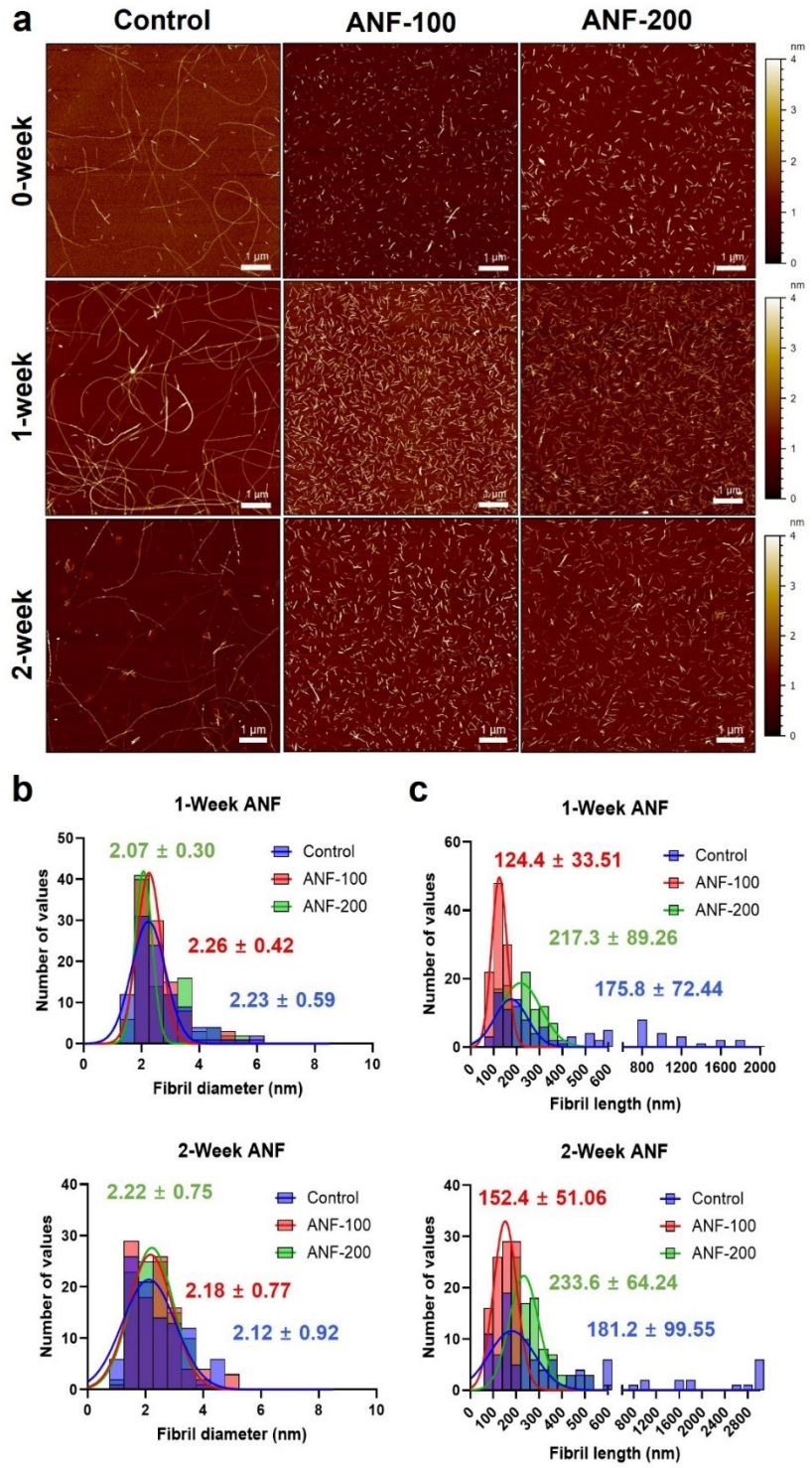

Figure S11. AFM analysis of uniformly truncated amyloid nanofibrils incubated at 24°C over 1 and 2 weeks. (a) AFM images of amyloid nanofibrils in the control group (untreated, left), ANF-100 (middle), and ANF-200 (right) after incubation at 24°C for 0, 1, and 2 weeks, showing no significant elongation, indicating stability of the truncated nanofibrils at this temperature. (b, c) Histograms displaying diameter (b) and length (c) measurements, fitted to a Gaussian model, with calculated mean and standard deviation values. Quantitative analysis was based on 100 measurements per condition.

Table S1. Summary of periodic pitch measurements for various amyloid nanofibrils from the literature[1-4]

Amyloid Type	Pitch	Method
Alzheimer's Aβ1-42	460 Å	Cryo-EM
β-Lactoglobulin	35–61 nm 75–135 nm 100–255 nm (2, 3, and 4 strands)	AFM
RIPK3	23 nm	AFM, Cryo-EM, ssNMR
α-Synuclein	92–194 nm	AFM, Cryo-EM, ssNMR
PHF	62.8 nm	Cryo-EM
Amyloid light chain	53.2 nm	Cryo-EM

References

1. R. Zhang, X. Hu, H. Khant, S. J. Ludtke, W. Chiu, M. F. Schmid, C. Frieden and J.-M. Lee, *Proceedings of the National Academy of Sciences*, 2009, **106**, 4653-4658.

2. J. Adamcik and R. Mezzenga, *Soft Matter*, 2011, **7**, 5437-5443.

3. X. Wu, Y. Ma, K. Zhao, J. Zhang, Y. Sun, Y. Li, X. Dong, H. Hu, J. Liu, J. Wang, X. Zhang, B. Li, H. Wang, D. Li, B. Sun, J. Lu and C. Liu, *Proceedings of the National Academy of Sciences*, 2021, **118**, e2022933118.

4. U. Cendrowska, P. J. Silva, N. Ait-Bouziad, M. Müller, Z. P. Guven, S. Vieweg, A. Chiki, L. Radamaker, S. T. Kumar, M. Fändrich, F. Tavanti, M. C. Menziani, A. Alexander-Katz, F. Stellacci and H. A. Lashuel, *Proceedings of the National Academy of Sciences*, 2020, **117**, 6866-6874.